A slenderness based method for web crippling design of aluminium tubular sections

Marina Bock[1*], Shashank Gupta[2], Mostafa Fahmi Hassanein[3] and Yong Sheng[4]

[1]Dr, Senior lecturer in Structural Engineering, School of Architecture and Built Environment, University of Wolverhampton, Wolverhampton, WV10 0JP, UK, marina.bock@wlv.ac.uk

[2]Dr, Senior lecturer in Structural Engineering, School of Architecture and Built Environment, University of Wolverhampton, Wolverhampton, WV10 0JP, UK, shashank.gupta@wlv.ac.uk

[3]Prof, Professor of Structural Engineering Department of Structural Engineering, Faculty of Engineering, Tanta University, Tanta, Egypt, mostafa.fahmi@f-eng.tanta.edu.eg

[4]Prof, Professor of Structural Engineering, School of Architecture and Built Environment, University of Wolverhampton, Wolverhampton, WV10 0JP, UK, y.sheng2@wlv.ac.uk

Abstract

Existing web crippling design provisions available in European, American and Australian/New Zealand standards are based on empiric equations that differ from the approach adopted for the treatment of other instabilities such as local or overall buckling which employ χ-λ curves. Assessment of those empiric web crippling provisions based on test data available in the literature and reported herein for Interior-One-Flange (IOF) and Interior-Two-Flange (ITF) loading conditions has demonstrated that they provide unsafe and inconsistent predictions thereby highlighting the need to develop an alternative approach. Focusing on aluminium tubular sections subjected to IOF and ITF loading conditions, this article reports experimental and numerical results that were used to develop χ-λ curves for web crippling design. The tubular sections were made of 6060 and 6063-T6 aluminium alloys and were manufactured by extrusion. A total number of twelve tests were carried out and subsequently used to develop and calibrate a numerical model. The measured dimensions, material properties and web

crippling loads attained are reported. After successful calibration of the numerical model, parametric studies covering a wide range of slenderness and support lengths were carried out. In order to derive the χ-λ approach three numerical analysis were performed as part of the parametric study: (i) a linear elastic analysis; (ii) a plastic analyses; and (iii) a geometrical and material non linear analysis. A total number of 288 numerical results were used to derive the new method. Compared with European, American and Australian/New Zealand standards, the derived χ-λ design method provides more accurate and reliable predictions for web crippling of aluminium tubular sections.

1. Introduction

Web crippling is a phenomenon that develops in metallic structures subjected to concentrated transverse forces. The transverse force compresses the webs of the cross-section, which might consequently yield, buckle or yield and buckle simultaneously depending on the cross-section shape and web slenderness. There are four possible web crippling load conditions as defined in the North American Specification NAS (2001) and the AS/NZS 1664.1 (1997) namely Interior-One-Flange (IOF), Interior-Two-Flange (ITF), Exterior-One-Flange (ETF) and Exterior-Two-Flange (ETF). They are all depicted in Figure 1 where s_s is the length over which the transverse load is applied commonly referred to as bearing length and h_w is the high of the web, see Figure 2. These load conditions were first defined by Winter and Pian (1946) in the first web crippling experimental investigation reported in the literature.

There is extensive research available on web crippling performance of cross-sections made of cold-formed steel and stainless steel, however, the amount of web crippling studies on aluminium alloys is less extensive. With aluminium becoming more popular in the construction industry due to its lightweight properties, corrosion resistance and high strength to weight ratio, their structural performance needs to be further investigated to ultimately explore further applications. Particular attention must be placed upon the fact that its Young's modulus is one third of steel's which makes aluminium structures more susceptible to deflections and instabilities including web crippling.

The first web crippling investigation on aluminium sections found in the literature was carried out by Tryland et al. (1999). I-section and SHS extrusions were tested under the IOF and EOF load conditions to generate well documented experimental data. Repeated tests rotating extrusions about their longitudinal axis as well as bearing lengths with circular and squared shapes were also taken into consideration. Later on, Zhou and Young (2008) reported a wide experimental programme on SHS and RHS under ITF and ETF load conditions. The experimental data were used to find strength-to-yield stress ratios for normal and high strength alloys and assess the impact of the bearing length on the web crippling strength. It was found that high strength alloys can achieve web crippling resistances 20% higher than normal alloys and that the influence of the bearing length (i.e. the length over which the transverse load is applied) on the web crippling resistance is higher for ETF loading than for ITF. In the companion paper, Young and Zhou (2008) used their previous data from Zhou and Young (2008) to assess the NAS (2001), AS/NZS 1664.1 (1997), AA (2005) and EN 1999-1-1 (2000) and developed unified empirical equations for ITF and ETF that showed improved web crippling predictions. Their equations follow the same empirical principle of the design provisions given in NAS (2001). In Zhou et al. (2009), the same team of researchers undertook another experimental programme on SHS and RHS extrusions subjected to End Loading (EL) and Interior Loading (IL) which are alternative loading conditions where the specimens lay over a continuous rigid bed that were first proposed by Zhao and Hancock (1992). Zhou and Young (2010) also investigated the influence of perforations in SHS and RHS extrusions subjected to ETF and ITF loading while Chen et al. (2015) derived new empirical equations for all four loading cases. Su and Young (2018) conducted tests on stocky SHS and RHS and proposed a new design methodology based on the continuous strength method (CSM) (Gardner 2008, Afshan and Gardner 2013, Bock et al. 2015 and Su et al. 2015). Alsanat et al. (2019) reported the first experimental programme on cold-formed aluminium C-sections and found that existing design provisions for both aluminium given by AS/NZS 1664.1 (1997) and cold-formed steel given by AS/NZS 4600 (2010) and by EN 1993-1-3 (2006) are unsuitable. Table 1 summarises existing research on web crippling of aluminium sections. As can be noted, to date current design guidelines and models proposed for web crippling design are based on empirical equations.

The present paper reports the results of an experimental programme on aluminium tubes subjected to IOF and ITF. The tubes were manufactured by extrusion with squared corners. The experimental results were combined with existing test data and used to assess existing design codes and standards. The assessment presented here showed, as other researchers have also highlighted, that existing web crippling provision are inaccurate and unreliable. This is mainly because existing web crippling provisions are fully empirical. The test results were then subsequently used to develop, carefully calibrate a numerical model and perform an extensive parametric study. The result of the parametric study were used to derive a new slenderness based method for web crippling design employing strength curves which is the same approach used for the treatment of other buckling instabilities such as local, overall buckling and patch loading. Past studies have proved that slenderness based approaches are possible for web crippling design and provide more reliable predictions (Duarte and Silvestre 2013, Bock and Real 2014, Almatrafi et al. 2021, Zhao and Hancock 1995, Nguyen et al. 2017 and Nguyen et al. 2020).

2. Experimental programme

This section reports the material and web crippling tests carried out within the scope of this article. Details of the experiments follow below along with an assessment of existing design standards.

2.1 Description of the specimens

The specimens consisted of SHS/RHS extrusions made of aluminium grades 6063T6 and 6060 with nominal dimensions H×B×t of the overall height H, overall width B and thickness t of 50×50×3, 50×50×2 and 51×51×1.64 as depicted in Figure 2. A total number of twelve specimens were tested, 6 under IOF loading and 6 under ITF loading. The actual dimensions of each specimen were measured with a digital Vernier calliper and are reported in Table 2. This table also reports the flat portion of the web h_w (i.e. H-2t) to thickness ratio h_w/t. All tubes were delivered in lengths of 500 mm approximately and were cut at the laboratories of the University of Wolverhampton to the lengths L shown in Table 2 which are the minimum lengths that meet the definition of IOF and ITF loading given in the NAS (2001) and the AS/NZS 1664.1 (1997) for a bearing length s_s and support length of 50 mm. The material specification of the tubes as provided by the supplier is given in Table 3 where E is the Young's modulus, f_0 is the 0.2% proof strength and f_u is the ultimate stress.

2.2 Material coupon testing

Material coupon testing took place at the laboratories of the University of Birmingham in accordance with the EN ISO 6892-1:2016 (2016). Details of the coupons and testing methodology are available in Bock et al. (2021), an article on biaxial bending of aluminium tubes. Six coupon test results from Bock et al. (2021) were relevant to the scope of the present research. All six coupons showed a Ramberg-Osgood non-linear stress-strain relationship with marginal strain hardening, see Figure 3, with properties summarised in Table 4, where t is the measured thickness of the coupon, E is the Young's modulus, f_0 is the 0.2% proof strength, n is the Ramberg-Osgood exponent, f_u is the ultimate stress and ε_u is the strain at ultimate stress. The cross-sectional material properties were based on mean values of each pair of coupon test results.

2.3 Web crippling tests

A total number of twelve web crippling tests were conducted, six of which were repeated tests under IOF and six were repeated under ITF loading at the laboratories of the University of Wolverhampton. The loads were applied by means of 50 mm thick steel bearing plates with a bearing length s_s of 50 mm. All the bearing plates were manufactured to load the full width of the tube and were allowed to rotate as shown by the test set ups presented in Fig. 4. The flanges of the tubes were not fastened to the bearing plates. In the IOF loading test, the load was applied at mid-span over the bearing length and blocks made of engineered wood (Bock and Real 2014) were inserted in the tubes at the supports, which were 50 mm long, to ensure that web crippling failure occurs under the bearing length only. In the ITF loading tests, two identical bearings with a length s_s of 50 mm were positioned at mid lengths of each specimen. The transverse load was applied by a 100 kN Zwick Roell testing frame incorporating load cells under the hydraulic jack. Displacement control was used to drive the machine at a rate of 0.5mm/min. The load readings and machine's crosshead vertical displacement were logged at 1 s intervals.

All specimens failed by web crippling under the bearing length some of which are shown in Figure 5 while Table 6 presents the ultimate experimental load $R_{w,u,test}$ achieved by the specimens.

2.4 Assessment of existing standards

The experimental data generated within the scope of this article have been complemented with all existing tests from the literature on SHS/RHS tested under IOF (Tryland et al. 1999, Zhou and Young 2008, Chen et al. 2015 and Su and Young 2018) and ITF (Zhou and Young 2008, Chen et al. 2015 and Su and Young 2018) loading to assess existing design standards for structural aluminium that include a web crippling provision. The design standards taken into consideration were:

(i) the unified equation from the NAS (2001) given by Eq. (1) with coefficients C, C_R, C_N and C_h. Note that NAS (2001) does not provide coefficients for SHS/RHS and therefore, coefficients for channels for IOF loading and hat sections for ITF loading were used as they provided the best agreement with test data.

$$R_{w,Rd,NAS} = Ct^2 f_0 \sin\phi \left(1 - C_R\sqrt{\frac{r}{t}}\right)\left(1 + C_N\sqrt{\frac{s_s}{t}}\right)\left(1 - C_h\sqrt{\frac{h}{t}}\right) \quad (1)$$

(ii) the equations from AA (2005) given by Eqs (2) and (3) for Interior and Exterior loading, respectively, where C_{w1} = 140 mm, C_{w2} = 33 mm and C_{w2} = 10 mm with coefficients C_{wa} and C_{wb} given by Eqs (4) and (5). Both equations are reported herein for completeness albeit only Eq (5) was used in the present assessment.

$$R_{w,Rd,AA} = C_{wa}(s_s + C_{w1})/C_{wb} \text{ for Interior Loading} \quad (2)$$

$$R_{w,Rd,AA} = 1.2C_{wa}(s_s + C_{w2})/C_{wb} \text{ for Exterior Loading} \quad (3)$$

$$C_{wa} = t^2 \sin\theta \left(0.46f_0 + 0.02\sqrt{Ef_0}\right) \quad (4)$$

$$C_{wb} = C_{w3} + r(1 - \cos\phi) \quad (5)$$

(iii) the design approach from the EN 1999-1-1 (2000) given by Eqs. (6)-(14). This approach is currently applicable to plate girders and therefore the original nomenclature has been adapted to SHS/RHS. In this method a is the distance between transverse stiffeners taken as the full length of the specimen L if no stiffeners are provided.

$$R_{w,Rd,EN1999-1-1} = \chi_F l_y t f_0 / \gamma_{M1} \quad (6)$$

$$\chi_F = 0.5/\lambda_F \quad (7)$$

$$\lambda_F = \sqrt{l_y t f_0 / F_{cr}} \quad (8)$$

$$F_{cr} = 0.9 k_F E t^3 / h_w \quad (9)$$

$$k_F = 6 + 2(h_w/a)^2 \text{ for IOF loading} \quad (10)$$

$$k_F = 3.5 + 2(h_w/a)^2 \text{for ITF loading} \quad (11)$$

$$l_y = s_s + 2t\left(1 + \sqrt{m_1 + m_2}\right)\ but\ l_y \leq a\ for\ IOF\ and\ ITF \quad (12)$$

$$m_1 = B/t \quad (13)$$

$$m_2 = 0.02(h_w/t)^2\ if\ \lambda_F > 0.5 \text{ otherwise } m_2 = 0 \quad (14)$$

(iv) the procedure given in EN 1993-1-3 (2006) for cold-formed steel which has also been adopted in EN 1999-1-4 (2009), the part for cold-formed structural sheeting, given by Eq. (15). In this equation the value of α depends on the clear distance e between two opposing transverse loads (i.e. the support and the applied load). For $e \leq 1.5h_w$ $\alpha=0.075$ while for $e > 1.5h_w$ $\alpha=0.15$ and as a general rule the former applies to ITF loading and the latter to IOF loading. EN 1999-1-4 (2009) refers to cases where $e \leq 1.5h_w$ as Category 1 and cases of $e > 1.5h_w$ as Category 2. For Category 1 $l_a=s_s$ but ≤40 mm while for Category 2 $l_a=s_s$ for symmetric cases where the transverse shear force on either side of the transverse load is the same.

$$R_{w,Rd,EN1999-1-4} = \alpha t^2 \sqrt{f_o E}\left(1 - 0.1\sqrt{r/t}\right)\left(0.5 + \sqrt{0.02\, l_a/t}\right)(2.4 + (\phi/90)^2)/\gamma_{M1} \quad (15)$$

In Eqs (1), (5) and (15) r is the internal bend radius of the corners of the cross-section taken as 0 for extruded sections as the corners are squared. For the assessment, all partial safety factors γ_{M1} were set to one and the predicted values by Eqs (1-3), (6) and (15), which provide the resistance per web, were multiplied by the number of webs of the cross-section (i.e. 2). The results are presented in Figures 6 and 7 for IOF and ITF loading respectively, where the experimental ($R_{w,exp}$) to predicted ratio ($R_{w,pred}$) is plotted against the slenderness ratio h_w/t. The assessment shows data falling both on the safe side (i.e $R_{w,exp}/R_{w,pred}>1$) and the unsafe side with high scatter highlighting the need for an alternative approach to web crippling design. Statistical results are presented in Table 5, with regards to mean and coefficient of variation (COV), which show that EN 1999-1-4 (2009) provides little agreement with experimental data for both IOF and ITF loading. The most accurate provision is that given by AA (2005) for IOF loading and NAS (2001) for ITF loading. It is also noted for ITF loading, EN 1999-1-1 (2000) shows less scatter but higher mean (i.e. more conservative). These results strengthen the need to develop an alternative approach for web crippling design.

3. Finite Element modelling

The finite element (FE) software package Simulia Abaqus 2020 was used to simulate the structural behaviour of aluminium alloy tubes subjected to web crippling under the IOF and ITF loading conditions. Further details about the modelling approach to simulate web crippling are provided in this section

3.1 Geometry discretization

The geometry of the tubes was modelled by using 3D deformable shell elements and discretised using the doubly curved four-noded shell elements with reduced integration S4R. This element has six degrees of freedom at each node and has been successfully used in modelling of web crippling behaviour of aluminium tubes (Zhou and Young 2010, Chen et al 2015, Su and Young 2018 and Castaldo et al. 2016). The cross-section size was based on centreline dimensions h × b, see Figure 2. Due to symmetry about the vertical axis for both IOF and ITF loading, half of the tube was modelled. A mesh convergence study was also performed which revealed that an element size of 2 mm × 2 mm provides accurate modelling results within reasonable computational time.

3.2 Material modelling

The FE models incorporated both elastic and plastic parts of the stress-strain curve. The elastic part was modelled by the measured Young's modulus E and using a Poisson's ratio coefficient of 0.33. For the plastic part, the measured stress σ_{nom} and strain ε_{nom} were converted into true stress (σ_{true}) and true plastic strain ($\varepsilon_{pl,true}$) by using Eq (16) and Eq. (17), respectively, and subsequently incorporated into the models. Isotropic behaviour was specified.

$$\sigma_{true} = \sigma_{nom}(1 + \varepsilon_{nom}) \tag{16}$$

$$\varepsilon_{pl,true} = ln(1 + \varepsilon_{nom}) - \frac{\sigma_{true}}{E} \tag{17}$$

3.3 Boundary conditions and interactions

The boundary conditions implemented in the numerical model were the same as those used in the tests. All supporting plates and bearing lengths were modelled by using 3D analytical rigid shells. Reference points (RPs) located in the centre were assigned to all rigid shells to which boundary conditions were applied as shown in Figures 8 and 9 for IOF and ITF, respectively. In these figures U1, U2 and U3 are displacements corresponding to the x, y and z directions respectively while UR1, UR2 and UR3 are rotations about the x-x, the y-y and z-z axes.

For IOF loading models the supports were allowed to rotate about the cross-sectional horizontal axis only and the rest degrees of freedom were restrained. At one of the ends, the longitudinal displacement was also allowed. All degrees of freedom were restrained at the reference point of the bearing length except vertical displacement.

For ITF loading models, all degrees of freedom of the bottom bearing plate were restrained while only vertical displacement was allowed at the top bearing plate.

In both IOF and ITF loading, surface-to-surface contact interaction was applied to the regions of the tube in contact with the bearing lengths and supports as shown in Figures 8 and 9. The 3D rigid plates were defined as “Master surface” while the regions of the tube in contact were defined as “Slave surface”. Contact was modelled by using hard normal behaviour and penalty isotropic tangential behaviour with a friction coefficient of 0.6. The element thickness of the tube was excluded and adjustment of the slave surface was allowed only to remove overclosure.

To apply the load in the FE models, a vertical displacement was defined at the RPs. To solve the models, the general static method in two steps allowing for geometric nonlinearities was used. The vertical displacements introduced in the first and second step were 0.1 mm and 20, respectively. It was observed that introducing the displacement in two steps removed numerical convergence issues. Like in other numerical web crippling investigations, initial imperfections or residual stresses were not modelled as they do not have any effect on the web crippling response (Ren et al. 2006, Zhou and Young 2007 and Bock et al. 2013).

3.4 Validation of the numerical model

The reliability of the FE model was assessed by comparing the experimental and numerical ultimate loads and failure modes. The failure modes achieved by the models are shown in Figure 10 where it is observed that they replicate the same failure modes achieved during testing shown in Figure 5. Table 6 presents the ultimate experimental load $R_{w,u,test}$, the ultimate numerical to test load ratio $R_{w,u,FE}$/ $R_{w,u,test}$ as well as the mean value for that ratio and coefficient of variation. The comparison shows a mean ratio very close to one and relatively small COV for both IOF and ITF loading models thereby enabling to conclude that the developed numerical model is accurate and reliable.

3.5 Parametric studies

Following validation of the developed numerical model, parametric studies were carried out in order to extend structural performance data on aluminium SHS/RHS subjected to IOF and ITF web crippling loading conditions. Two geometries namely SHS and RHS, four thicknesses, three bearing lengths and two alloys were considered. The centreline dimensions h × b for SHS and RHS were 50 × 50 and 100 × 50, respectively, while the thicknesses were 5 mm, 3 mm, 2 mm and 1 mm. The ratio of h/t ranged therefore from 9 to 49. The bearing lengths were 25 mm, 50 mm and 75 mm. The length of SHS was 340 mm and 240 mm for IOF and ITF loading respectively, while RHS were 490 and 390 mm long for IOF and ITL loading, respectively. The aluminium alloys considered had the following material properties: (i) E = 66 GPa, f_0 = 300 MPa, n=35, f_u = 339 MPa and ε_u=0.084 and (ii) E = 67.55 GPa, f_0 = 198 MPa, n=28.5, f_u = 229 MPa and ε_u=0.078. Note that these material properties were also used in Bock et al. (2021) and are based on average values of tensile coupon testing. The following section describes how these models were used to develop a new slenderness based approach for web crippling design of aluminium SHS/RHS.

4. Development of the slenderness based $\chi(\lambda)$ method

4.1 Basis of the method

Slenderness based or $\chi(\lambda)$ method is a design approach that finds the ultimate load by means of a strength curve χ that is a function of the slenderness λ as given by Eqs. (18) – (20) where A and B are dimensionless coefficients requiring calibration. On this basis, the ultimate web crippling load $R_{w,u}$ can therefore be found involving the buckling $R_{w,cr}$ and plastic $R_{w,pl}$ load. To determine $R_{w,u}$, $R_{w,cr}$ and $R_{w,pl}$ three types of numerical analyses were carried out on the geometries described in parametric studies section: (i) a material and geometrical non-linear analysis to obtain $R_{w,u}$, (ii) a linear elastic buckling analysis to obtain $R_{w,cr}$ and (iii) a first order plastic analysis (i.e. non linear material without considering geometrical nonlinearities) to obtain $R_{w,pl}$. Note that the elastic $R_{w,cr}$ and plastic $R_{w,pl}$ loads can only be determined numerically. A total number of 144 numerical results were generated and used to derive predictive models for $R_{w,cr}$, $R_{w,pl}$ and $\chi(\lambda)$ functions for both IOF and ITF loading.

$$R_{w,u} = \chi R_{w,pl} \tag{18}$$

$$\chi = \frac{A}{\bar{\lambda}^B} \leq 1 \tag{19}$$

$$\lambda = \sqrt{\frac{R_{w,pl}}{R_{w,cr}}} \tag{20}$$

4.2 Linear elastic buckling analysis

Linear elastic analyses were performed to obtain buckling shapes and associated eigenvalues. The load taken as the critical buckling load $R_{w,cr}$ was the lowest elastic buckling load pertinent to web buckling. Because contact interaction is incompatible with buckling analysis, for IOF models the interaction between the specimen and supporting plates was simulated by using tie type constraint and the bearing plate was simulated with a pressure load. For ITF models, the interaction between the bearing plates and specimen was simulated by using tie type constraint and the load as a concentrated force applied at the reference point of the top bearing plate. To obtain $R_{w,cr}$ the lowest eigenvalue pertinent to web buckling was multiplied by the value of the applied load. Note that for IOF loading, the total magnitude of the pressure load was used. Some examples of web buckling modes are shown in Figures 11 and 12 for bearing lengths of

25 and 75 mm, respectively, which indicate that the web buckling shape does not significantly change with varying bearing length.

The numerical results from linear elastic buckling analyses $R_{w,cr,FE}$ were used to derive an analytical model that predicts the elastic buckling load $R_{w,cr}$. The model namely $R_{w,cr,pred}$ is given in Eq. (21) which is stems from classical elastic theory of instability of a plate loaded with a concentrated in-plane force at the edge where the dimensionless buckling coefficient k_F may be derived for a given plate geometry with certain boundary conditions. Same approach was also used in Bock and Real (2014) and Almatrafi et al. (2021). Coefficients k_F were therefore derived herein by using multilinear regression analysis considering relevant geometrical variables and are given by Eqs. (22) and (23) for IOF and ITF, respectively. A graphical comparison between predicted and numerical values is presented in Figure 13 with statistics given in Table 7. The comparison shows excellent agreement between numerical and predicted data with mean values close to unity and reasonable COVs. Note that the predictive models given in Eqs. (21) and (22) provide the elastic buckling load of the cross-section and not of a single web.

$$R_{w,cr,pred} = k_F \frac{\pi^2 E t^3}{12(1-\nu^2)h} \tag{21}$$

For IOF loading (22)

$$k_F = 0.003\, h/b + 0.006\, s_s/h + 4.3 \times 10^{-6}\, s_s/t - 0.008\, t/h - 0.114(s_s/L)^2$$

For ITF loading (23)

$$k_F = 0.134\, s_s/L + 1.24 \times 10^{-5}\, s_s/t - 0.7(s_s/L)^2 + 0.004(s_s/h)^2 + (s_s/L)^3$$

4.3 First order plastic analysis

The modelling assumptions used to obtain the web crippling ultimate load $R_{w,u}$, apart from geometrical nonlinearities, were adopted in first-order plastic analysis to obtain the plastic load $R_{w,pl}$. The load – displacement response obtained from first order plastic analysis is shown in Figure 14 for some specimens whilst highlighting the influence of the bearing length and aspect ratio. The plotted displacement corresponds to the vertical translation of the centre of the top flange at midspan (i.e. where the RP was defined). From Figure 10 (b) it is observed that the plastic load achieved by SHS is the same as its RHS counterpart. In addition to this, most of curves did not reach a clear, well-defined maximum and kept increasing with reducing slope. Same trend was observed in past studies on other cross-sections and materials (Duarte and Silvestre 2013, Bock and Real 2014 and Almatrafi et al. 2021). To obtain the plastic load $R_{w,pl}$, the graphical method proposed by Dos Santos et al. (2018) was used which assumes that the plastic load is attained when the slope of the load-deflection curve is 1% of the initial stiffness. Other graphical methods to determine plastic loads are also available such as the Southwell plot (Southwell 1932), the convergence indicator plot (Horne and Merchant 1965) and the tangent stiffness plot (Doerich and Rotter 2011), which were found to provide similar predictions to Dos Santos et al. (2018). Some plastic mechanism developed are shown in Figure 15.

The numerical results from plastic analyses $R_{w,pl,FE}$ were used to derive an analytical model that predicts the plastic load $R_{w,pl}$. The model namely $R_{w,pl,pred}$ is given in Eq.(24) which is similar to the model employed by EN 1999-1-1 (2000) to predict plastic loads in the provision dealing with concentrated transverse forces which is based on plastic line theory. It is worth pointing out that this model does not contain the internal radius r and that other models for plastic loads are available for cross-sections with rounded corners and materials such as cold formed channels (Duarte and Silvestre 2013), stainless steel hat sections (Bock and Real 2014), cold-formed sigma sections (Almatrafi et al. 2021), cold-formed SHS and RHS (Zhao and Hancock 1995) and cold-formed lipped channels (Nguyen et al. 2020). In Eq. (24), l_y is the yield-prone effectively loaded length that can be calibrated from geometrical and mechanical properties. Equations for l_y were derived by using multilinear regression analysis considering relevant geometrical variables for IOF and ITF loading and are given by Eqs. (25) and (26), respectively. A graphical comparison between predicted and numerical values is presented in Figure 16 with statistics given in Table 7. As can be seen, the comparison shows excellent agreement between numerical and predicted data with mean values close to unity and reasonable COVs. Note the predictive models given in Eqs. (25) and (26) provide the plastic load of the cross-section and not of a single web.

$$R_{w,pl,pred} = l_y t f_0 \tag{24}$$

For IOF loading

$$l_y = 2.22 s_s + 0.92h + 25.82\, b/h + 1.16t + 0.52\, b/t - 613.80\, s_s/L - 0.65\, h/t \leq L \tag{25}$$

For ITF loading

$$l_y = 2.73 s_s + 0.54h + 46.59\, b/h - 0.044\, h/t - 1.11\, b/t + 1.73\, s_s/t \leq L \tag{26}$$

4.4 Proposed slenderness based $\chi(\lambda)$ equations for IOF and ITF

Having obtained the ultimate web crippling load $R_{w,u}$, the buckling load $R_{w,cr}$ and plastic load $R_{w,pl}$ numerically, the resulting χ-λ plot shown in Figure 17 for (a) IOF and (b) ITF loading was obtained and first slenderness $\chi(\lambda)$ based equations were derived by using regression analysis. Figure 17 also shows available curves for cold formed (CF) channels (Duarte and Silvestre 2013) and cold-formed sigma sections (Almatrafi et al. 2021) as well as stainless steel hat sections (Bock and Real 2014). Note that other $\chi(\lambda)$ curves with similar coefficients are also available in Nguyen et al. (2020) for cold-formed lipped channels but have not been added in Figure 17 for simplicity. The results show for IOF loading that the data follows a trend whereby χ slowly decreases with increasing λ following an exponential law and with low scatter. For ITF loading a family of χ-λ curves is observed for various s_s/h ratios. For both loading cases, it is observed that the proposed $\chi(\lambda)$ in Duarte and Silvestre (2013), Bock and Real (2014) and Almatrafi et al. (2021) are not suitable for extruded aluminium SHS/RHS. The results also show that SHS/RHS aluminium sections achieve a higher χ-λ relationship for IOF loading than existing data on other sections (i.e. channels, sigma sections and hat sections) and materials (i.e. stainless steel and cold-formed steel).

The $\chi(\lambda)$ curves shown in Figure 17 are the best fit trend lines that could be used to predict ultimate web crippling loads $R_{w,u}$ of any aluminium SHS/RHS when elastic buckling $R_{w,cr}$ and plastic $R_{w,pl}$ loads are determined numerically. As predictive models for these loads have been developed in sections 4.2 and 4.3, the final proposed $\chi(\lambda)$ curves incorporating $R_{w,cr,pred}$ and $R_{w,pl,pred}$ from Eqs (21-26) are shown in Figure 18 and are given by Eqs. (27) and (28). Note that for ITF loading, $\chi(\lambda)$ is expressed as a continuous function of s_s/h where coefficients A and B from the general form as given in Eq. (1), have been substituted by the best fit lines shown in Figure 19. Figure 18 shows that after the incorporation of the derived predictive models, the χ-λ values do not change significantly and best fit trend lines are very similar to those based on numerical values.

For IOF loading

$$\chi = \frac{1.03}{e^{0.47\lambda}} \leq 1 \tag{27}$$

For ITF loading

$$\chi = \frac{0.338 + 0.079\, s_s/h}{\lambda^{0.863-0.056 s_s/h}} \leq 1 \tag{28}$$

5. Validation of the proposed χ(λ) method against test and FE data

Taking into consideration experimental data reported in (Zhou and Young 2008, Chen et al. 2015 and Su and Young 2018) as well as tests and generated FE models presented herein, the proposed χ(λ) curves for IOF and ITF loading given in Eqs (27) and (28) used in conjunction with the derived models for the elastic critical load $R_{w,cr,pred}$ and plastic load $R_{w,pl,pred}$ as given by Eqs. (21)-(26) to determine the cross-sectional web crippling resistance $R_{w,u}$ are validated. To this end, the numerical $R_{w,u,FE}$ and experimental $R_{w,u,test}$ resistances of the cross-section were divided by the predicted values by the proposed method $R_{w,u,pred}$. Subsequently, mean and COV values of the ratios were determined for various data sets which are presented in Table 8. Compared to the statistics from the assessment of existing design standards presented in Table 5, it is observed that the mean and COV values of the predictions by the proposed method significantly improve. A graphical comparison between numerical/FE and predicted values is presented in Figure 20 showing that both experimental and FE data sets fall closer to the 45 degree line.

6. Conclusions

A series of tests have been performed on extruded aluminium SHS/RHS under IOF and ITF loading conditions. The test results were complemented with existing test data from literature (Tryland et al. 1999, Zhou and Young 2008, Chen et al. 2015 and Su and Young 2018) to show that the current standards for web crippling design for structural aluminium are very inaccurate and unreliable. The test results were also used to develop and calibrate a numerical model upon which to base the development of a slenderness based approach employing strength curves $\chi(\lambda)$ for web crippling design of extruded SHS/RHS underIOF and ITF loading. To achieve this, three types of analyses were undertaken: (i) a liner elastic analysis to determine critical loads $R_{w,cr}$, (ii) a first order plastic analysis considering perfect geometry and material nonlinearities to find plastic loads $R_{w,pl}$ and (iii) a full nonlinear analysis to obtain web crippling ultimate loads $R_{w,u.}$. It was found that sections with different aspect ratios h/b reach same plastic loads $R_{w,pl}$. The numerical values for $R_{w,cr}$ and $R_{w,pl}$ were used to derive the predictive models for such loads as presented in Eqs. (21)-(26) and find $\chi(\lambda)$ curves. χ and λ were found as shown by Eqs. (2) and (3). For IOF loading it was observed that a single $\chi(\lambda)$ could capture the data accurately, while for ITF loading a family of $\chi(\lambda)$ curves that depend on the s_s/h ratio would be needed. χ-λ values by using the developed predictive models from Eqs. (21)-(26) were finally used to accurately calibrate the $\chi(\lambda)$ curves given by Eqs. (27) and (28). The approach developed within the scope of this article has led to significantly improved and reliable predictions of the web crippling resistance of extruded aluminium SHS/RHS under IOF and ITF loading.

The research presented in this article has yet again proved that slenderness based approaches have potential to be adopted for web crippling design. Further research on additional cross-section shapes and materials is underway to extend this design approach.

Data Availability Statement

Some or all data, models, or code that support the findings of this study are available from the corresponding author upon reasonable request.

Acknowledgements

The research presented in this article has received funding from the Early Researcher Award Scheme 2018/19 of the University of Wolverhampton. The authors are also grateful to Mr Iain Liall and Paul Bates from the School of Engineering of the University of Wolverhampton for their assistance with the tests.

References

AA (Aluminium Association). 2005. *Aluminum design manual*. Washington, DC: The Aluminum Association.

Afshan, S. and Gardner, L. 2013. "The Continuous Strength Method for structural stainless steel design." *Thin-Walled Struct.* 68: 42-49.

Almatrafi, A., Theofanous, M., Bock, M. and Dirar, S. 2021. "Slenderness-based design for sigma sections subjected to interior one flange loading." *Thin-Walled Struct.* 158: 107194.

Alsanat, H., Gunalan, S., Guan, H., Keerthan, P. and Bull, J. 2019. "Experimental study of aluminium lipped channel sections subjected to web crippling under two flange load cases." *Thin-Walled Struct*. 141: 460-476.

AS/NZS 1664.1. 1997. *Aluminium structures—Part 1: limit state design*. Australian/New Zealand Standard AS/NZS 1664.1:1997. Sydney, Australia: Standards Australia.

AS/NZS 4600. 2010. *Cold-formed Steel Structures*. Australian/New Zealand Standard 4600:2010. Sydney, Australia: Standards Australia.

Bock, M. and Real, E. 2014. "Strength curves for web crippling design of cold-formed stainless steel hat sections." *Thin-Walled Struct*. 85: 93-105.

Bock, M., Arrayago, I., Real, E. and Mirambell, E. 2013. "Study of web crippling in ferritic stainless steel cold formed sections." *Thin-Walled Struct.* 69: 29-44.

Bock, M., Real, E. and Gardner, L. 2015. "Material and local buckling response of ferritic stainless steel sections." *Thin-Walled Struct*. 89: 131-141.

Bock, M., Theofanous, M., Dirar, S., Lipitkas, N. 2021. "Aluminium SHS and RHS subjected to biaxial bending: Experimental testing, modelling and design recommendations." *Eng. Struct.* 227: 111468.

Castaldo, P., Nastrib, E. and Piluso, V. 2016. "Evaluation of Rotation Capacity of RHS Aluminium Alloy Beams by FEM Simulation: Temper T6." *Key Eng. Mat*. 710: 281-287.

Chen, Y., Chen, X. and Wang, C. 2015. "Aluminum tubular sections subjected to web crippling." *Thin-Walled Struct*. 90: 49-60.

Doerich, C. and Rotter, J. 2011. "Accurate Determination of plastic collapse loads from finite element analyses." *Journal of Pressure Vessel Tech.* 133(1): 011202.

Dos Santos, G.B., Gardner, L. and Kucukler, M. 2018. "A method for the numerical derivation of plastic collapse loads." *Thin-Walled Struct.* 124: 258-277.

Duarte, A.P.C. and Silvestre, N. 2013. "A new slenderness-based approach for the web crippling design of plain channel steel beams." *Int. Journal of Steel Struct.* 3: 421-34.

EN 1993-1-3. 2006. *Eurocode 3: Design of steel Structures—Part 1.3: Cold-Formed Members and Sheeting.* European Committee for Standardization (CEN).

EN 1999-1-1. 2000. *Eurocode 9: Design of aluminum structures—Part 1.1: General rules—General rules and rules for buildings*. European Committee for Standardization (CEN).

EN 1999-1-4. 2009. *Eurocode 9: Design of aluminium Structures-Part 1.4: Cold-Formed structural sheeting*. European Committee for Standardization (CEN).

EN ISO 6892-1:2016. 2016. *Metallic materials — Tensile testing, Part 1: Method of test at room temperature*. London: BSI.

Gardner, L. 2008. "The continuous strength method." *Proceedings of the Institution of Civil Engineers-Structures and Buildings*. 161: 127-33.

Horne, M.R. and Merchant, W. 1965. *The Stability of Frames, vol. 9*. Oxford.

NAS (North American Specification). 2001. *North American Specification for the design of cold-formed steel structural members*. Washington, DC: American Iron and Steel Institute.

Nguyen, V.V., Hancock, G.J. and Pham, C.H. 2017. "New developments in the Direct Strength Method (DSM) for design of cold-formed steel sections under localised loading." *J. Struct. Eng*. 10 (3), 227–233.

Nguyen, V.V., Hancock, G.J. and Pham, C.H. 2020. "Consistent and Simplified Direct Strength Method for Design of Cold-Formed Steel Structural Members under Localised Loading." *J. Struct. Eng*. 146(6): 04020090.

Ren, W.X., Fang, S.E. and Young B. 2006. "Finite element simulation and design of cold-formed steel channels subjected to web crippling." *J. Struct. Eng*. 132: 1697–1975.

Southwell, R.V. 1932. "On the analysis of experimental observations in problems of elastic stability." *Proc. of the Royal Society a mathematical, physical and engineering science*. 135 (828): 601-616.

Su, M. N., Young, B. and Gardner, L. 2015. "The continuous strength method for the design of aluminium alloy structural elements." *Eng. Struct*. 122: 338–348.

Su, M.N. and Young, B. 2018. "Design of aluminium alloy stocky hollow sections subjected to concentrated transverse loads." *Thin-Walled Struct.* 124: 546–557.

Sundararajah, L., Mahendran, M. and Keerthan, P. 2017. "New design rules for lipped channel beams subject to web crippling under two-flange load cases." *Thin-Walled Struct.* 119: 421–437.

Tryland, B.T., Langseth, M. and Hopperstad, O.S. 1999. "Nonperfect aluminium beams subjected to concentrated loading." *J. Struct. Eng*. 125(8): 900–9.

Winter, G. and Pian, R.H.J. 1946. "Crushing strength of thin steel webs." *Engineering experiment station*, Bulletin no. 35, Part 1." New York, USA.

Young, B. and Zhou, F. 2008. "Aluminum tubular sections subjected to web crippling—Part II: Proposed design equations.", *Thin-Walled Struct*. 46(4): 352-361.

Zhao, X.L. and Hancock, G.J. 1992. "Square and rectangular hollow sections subjected to combined actions." *J. Struct. Eng*. 118:648-68.

Zhao, X.L. and Hancock, G.J. 1995. "Square and Rectangular Hollow Sections under Transverse End Bearing Force." *J. Struct. Eng*. 1323 – 1329.

Zhou, F. and Young, B. 2007. "Experimental and numerical investigations of cold-formed stainless steel tubular sections subjected to concentrated bearing load." *J. Constr. Steel Res*. 63 (11): 1452–1466.

Zhou, F. and Young, B. 2008. "Aluminum tubular sections subjected to web crippling—Part I." *Thin-Walled Struct*. 46(4): 339-351.

Zhou, F. and Young, B. 2010. "Web crippling of aluminium tubes with perforated webs." *Eng. Struct*. 32: 1397-1410.

Zhou, F., Young, B. and Zhao, X.L. 2009. "Tests and design of aluminum tubular sections subjected to concentrated bearing load.", *J. Struct. Eng*. 135 (7): 806–817.

Table 1. Relevant research on aluminium alloy sections subjected to web crippling

Reference	Section	Alloy	Load case	Relevant Contribution
Tryland et al. (1999)	SHS I-sec	AA6082-T6	26 IOF 26 EOF	Circular and rectangular bearings. Specimens were rotated about the longitudinal axis and tested three times. Investigation reports average values results.
Zhou and Young (2008)	RHS SHS	6063-T5 6061-T6	76 ETF 74 ITF	Testing and successful development of FE. Web slenderness from 6.3 to 74.5 was investigated. It was observed that the web crippling strength to yield stress ratio for 6063-T5 is 20% larger than for 6061-T6 and that the web crippling strength for ETF loading condition increases faster than those for ITF loading condition as the bearing length increases
Young and Zhou (2008)	RHS SHS	Aluminium 6063-T5 6061-T6	-	Development of two different unified equations based on experimental data. Assessment of NAS (2001), AS/NZS 1664.1 (1997), AA (2005) and EN 1999-1-1 (2000). It was observed that the web crippling strength is correlated to the N/h ratio where N is the bearing length and h is the depth of the flat portion of the web.
Zhou et al. (2009)	SHS	6061-T6	30 EL 34 IL	Assessment of the AA (2005) and EN 1999-1-1 (2000) which were found either unsafe or overly conservative. Critical values of web slenderness were also proposed beyond which web buckling governs. EL and IL loading first proposed in Zhao and Hancock (1992).
Zhou and Young (2010)	RHS SHS (with holes)	6063-T5 6061-T6	ETF ITF	Web crippling strength reduction factor equations were proposed for the ETF and ITF loading conditions. The effect of yield stress on the web buckling strength was also discussed in this paper.
Chen et al. (2015)	SHS	Not reported	12 IOF; 12 EOF 12 ITF; 12 ETF	Recalibration of existing web crippling design provisions for all load cases.
Su and Young (2018)	RHS SHS	6063-T5 6061-T6	6 IOF; 6 EOF 11 ITF; 11 ETF	Adaptation of the CSM for web crippling design of stocky tubular extrusions.
Alsanat et al. (2019)	C-sections	5052H36	20 ETF; 20 ITF	First experiments on cold-formed aluminium C-sections. Assessment of design standards for cold-formed steel and aluminium including AS/NZS 1664.1 (1997), AS/NZS 4600 (2010) and EN 1993-1-3 (2006) as well as Sundararajah et al. (2017) modifications for cold-formed steel channels. It was found that the design strengths predicted by the aforementioned specifications are unconservative and unsafe.

Table 2. Measured dimensions of the tested cross-sections

Cross-section	Test	Mill grade	H (mm)	B (mm)	t (mm)	h_w/t	L (mm)
50×50×3-1	IOF	6060	50.05	50.05	2.90	15.26	310
50×50×3-2	IOF	6060	50.06	50.06	2.91	15.20	310
50×50×2-1	IOF	6060	49.95	49.92	1.99	23.09	310
50×50×2-2	IOF	6060	49.95	49.92	1.99	23.09	310
51×51×1.64-1	IOF	6063T6	51.07	51.09	1.68	28.41	310
51×51×1.64-2	IOF	6063T6	51.06	51.08	1.68	28.40	310
50×50×3-1	ITF	6060	50.07	50.04	2.88	15.39	260
50×50×3-2	ITF	6060	50.05	50.05	2.88	15.38	260
50×50×2-1	ITF	6060	49.90	49.90	1.95	23.59	260
50×50×2-2	ITF	6060	49.95	49.95	1.95	23.62	260
51×51×1.64-1	ITF	6063T6	51.08	51.12	1.66	28.80	260
51×51×1.64-2	ITF	6063T6	51.09	51.15	1.66	28.81	260

Table 3. Material specification of the tubes

Cross-section	Mill grade	E (GPa)	f_0 (MPa)	f_u (MPa)
50×50×3	6060	70	170	260
50×50×2	6060	69.5	150	195
51×51×1.64	6063T6	69.5	170	215

Table 4. Relevant tensile coupon test results extracted from Bock et al. (2021)

Coupon	t (mm)	E (GPa)	f_0 (MPa)	n	f_u (MPa)	ε_u (%)
51×51×1.64-1	1.64	66.00	219	40	239	6.76
51×51×1.64-2	1.64	66.00	207	40	225	6.83
50×50×2-1	1.97	67.20	213	35	235	7.34
50×50×2-2	1.97	67.20	210	35	232	6.82
50×50×3-1	3.00	67.80	208	30	240	7.40
50×50×3-2	3.00	67.30	188	27	218	8.36

Table 5. Statistics of the assessment of existing web crippling provisions

Load case	**statistics**	**EN 1999-1-4 (2009)**	**EN 1999-1-1 (2000)**	**AA (2005)**	**NAS (2001)**
IOF	Mean	2.067	0.828	1.096	0.878
	COV	0.566	0.326	0.440	0.449
ITF	Mean	5.664	1.313	1.431	1.106
	COV	0.572	0.286	0.426	0.416

Table 6. Comparison between numerical and test results

	IOF		ITF	
Cross-section	$R_{w,u,test}$ (kN)	$R_{w,u,FE}$/ $R_{w,u,test}$	$R_{w,u,test}$ (kN)	$R_{w,u,FE}$/ $R_{w,u,test}$
50×50×3-1	50	0.95	73	0.99
50×50×3-2	49	0.98	73	0.99
50×50×2-1	31	0.95	41	1.06
50×50×2-2	31	0.96	42	1.04
51×51×1.64-1	27	0.97	34	0.90
51×51×1.64-2	26	1.00	33	0.91
Mean		0.97		0.98
COV		0.020		0.066

Table 7. Comparison between numerical values and derived predictive models

	IOF		ITF	
Statistics	$R_{w,cr,FE}$/ $R_{w,cr,pred}$	$R_{w,pl,FE}$/ $R_{w,pl,pred}$	$R_{w,cr,FE}$/ $R_{w,cr,pred}$	$R_{w,pl,FE}$/ $R_{w,pl,pred}$
Mean	0.99	0.99	0.96	0.99
COV	0.041	0.069	0.062	0.041

Table 8. Statistics of the validation against tests and FE results

	Data set	Sample size	Mean	COV
IOF	FE	51	0.94	0.133
	Tests	24	1.05	0.191
	FE+Tests	75	0.99	0.168
ITF	FE	51	1.01	0.110
	Tests	103	0.98	0.268
	FE+Tests	154	0.99	0.224

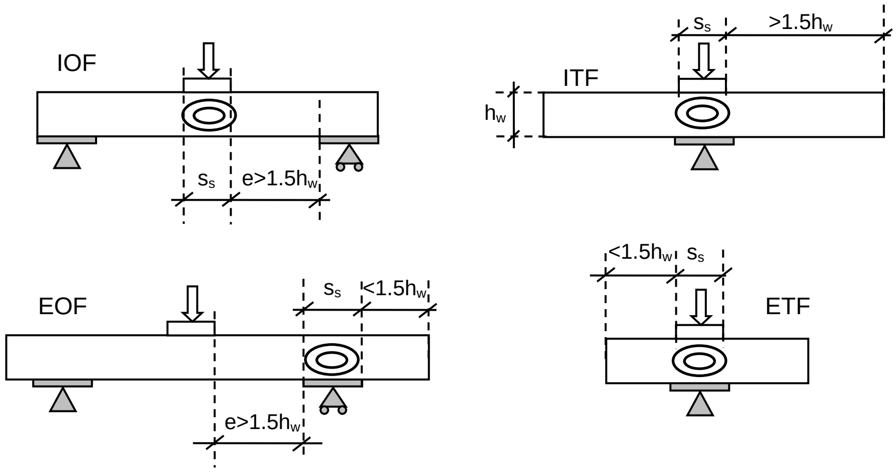

Figure 1. The four web crippling load conditions

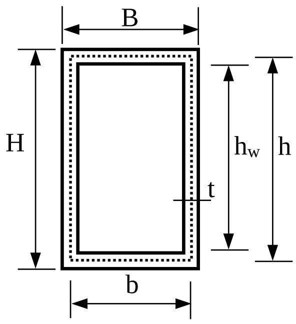

Figure 2. Cross-sectional notation

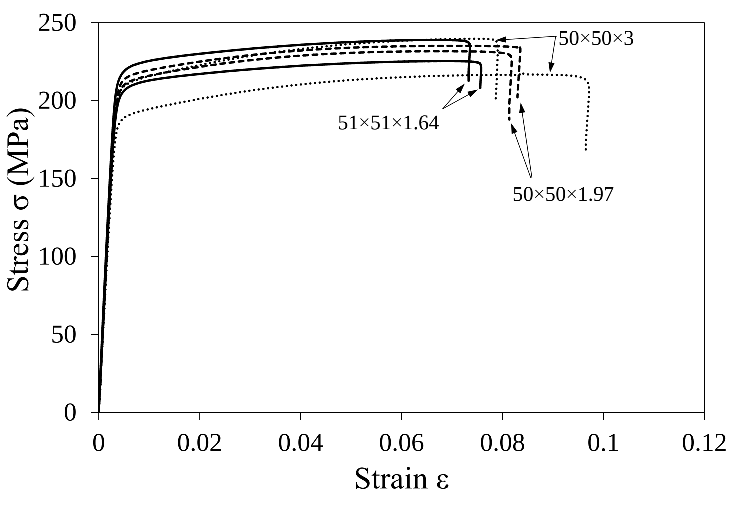

Figure 3. Material stress-strain relationship of tested coupons extracted from [90]

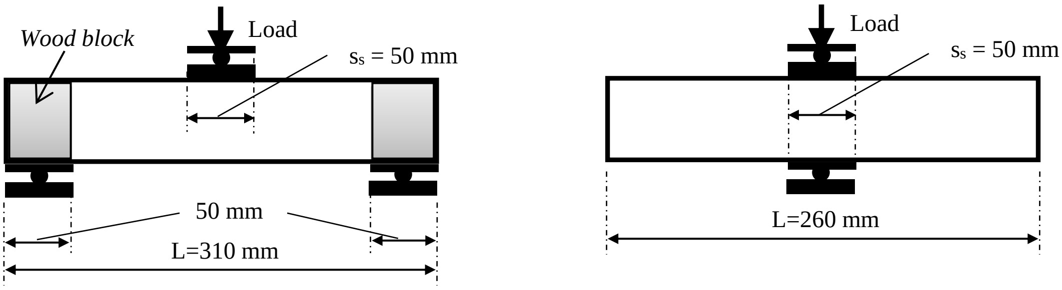

(a) (b)

Figure 4. IOF loading test set up (a) ITF loading test set up (b)

(a) (b)

Figure 5. Web crippling failure modes for (a) IOF loading and (b) ITF loading tests

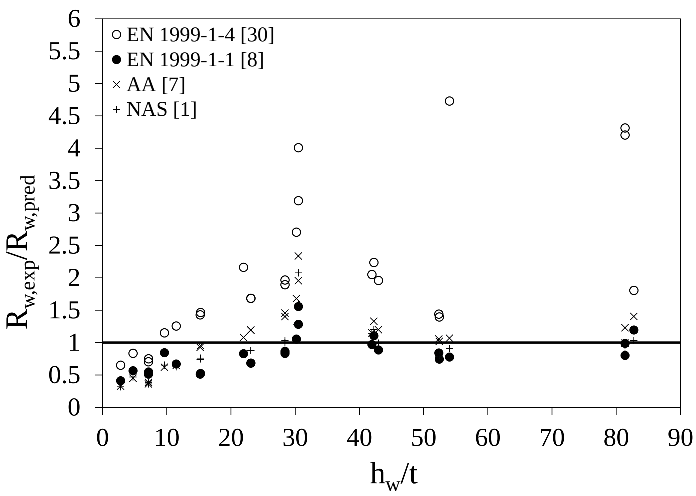

Figure 6. Assessment of existing design standards for IOF loading

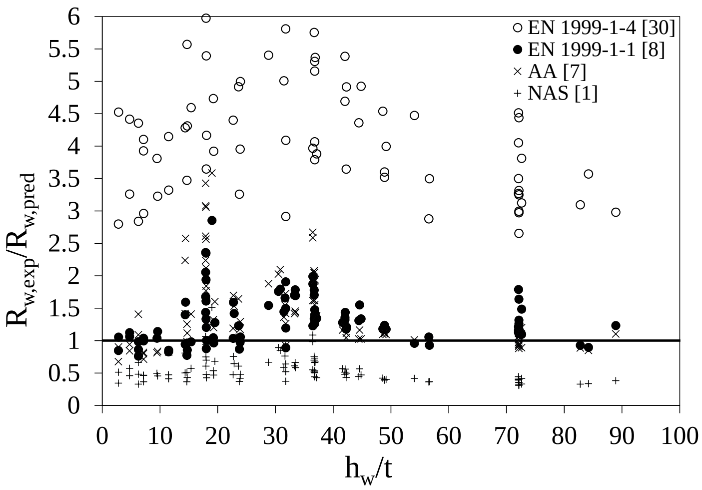

Figure 7. Assessment of existing design standards for ITF loading

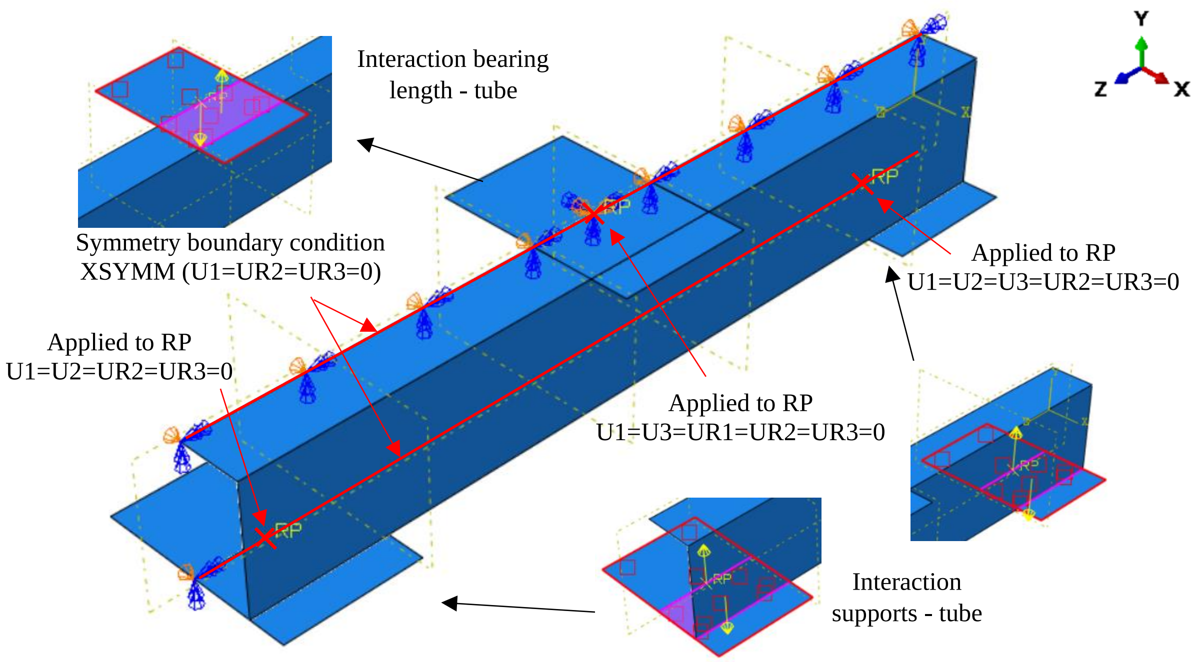

Figure 8. Interactions and boundary conditions of IOF loading models

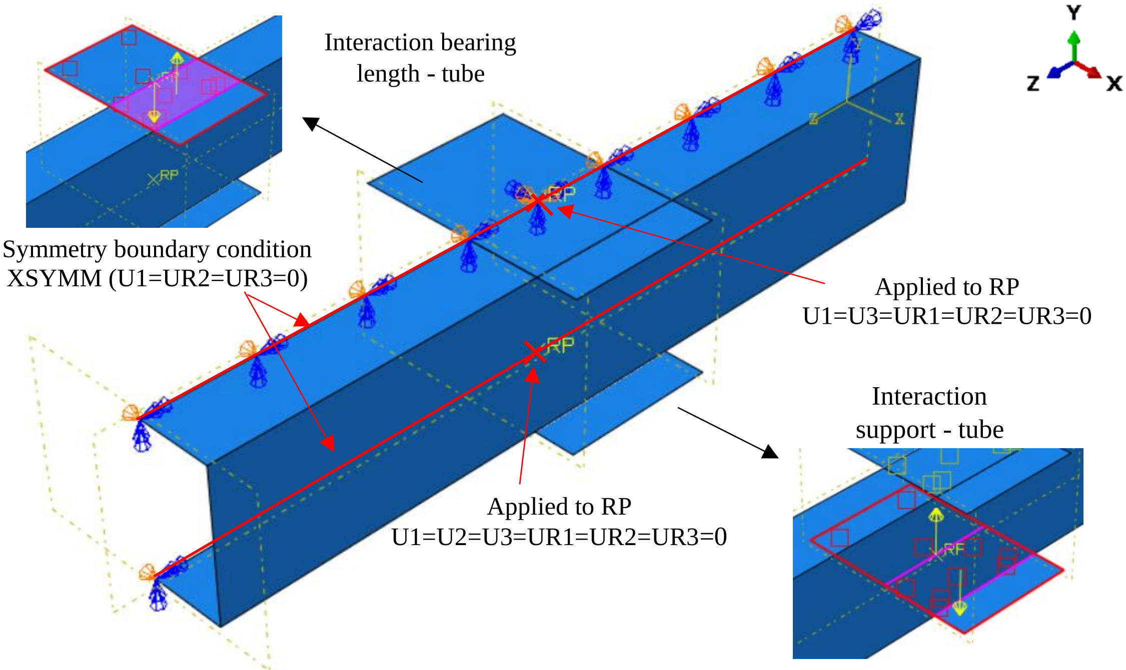

Figure 9. Interactions and boundary conditions of ITF loading models

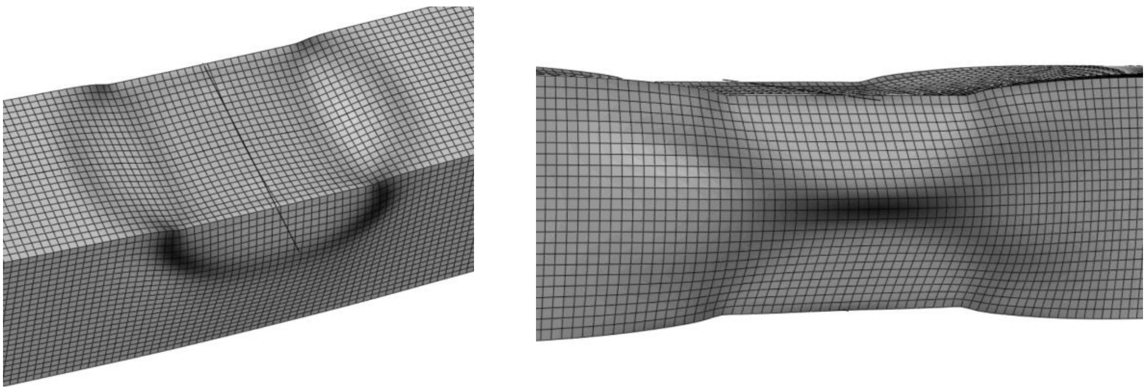

(a) (b)

Figure 10. Failure modes achieved by models for (a) IOF loading and (b) ITF loading

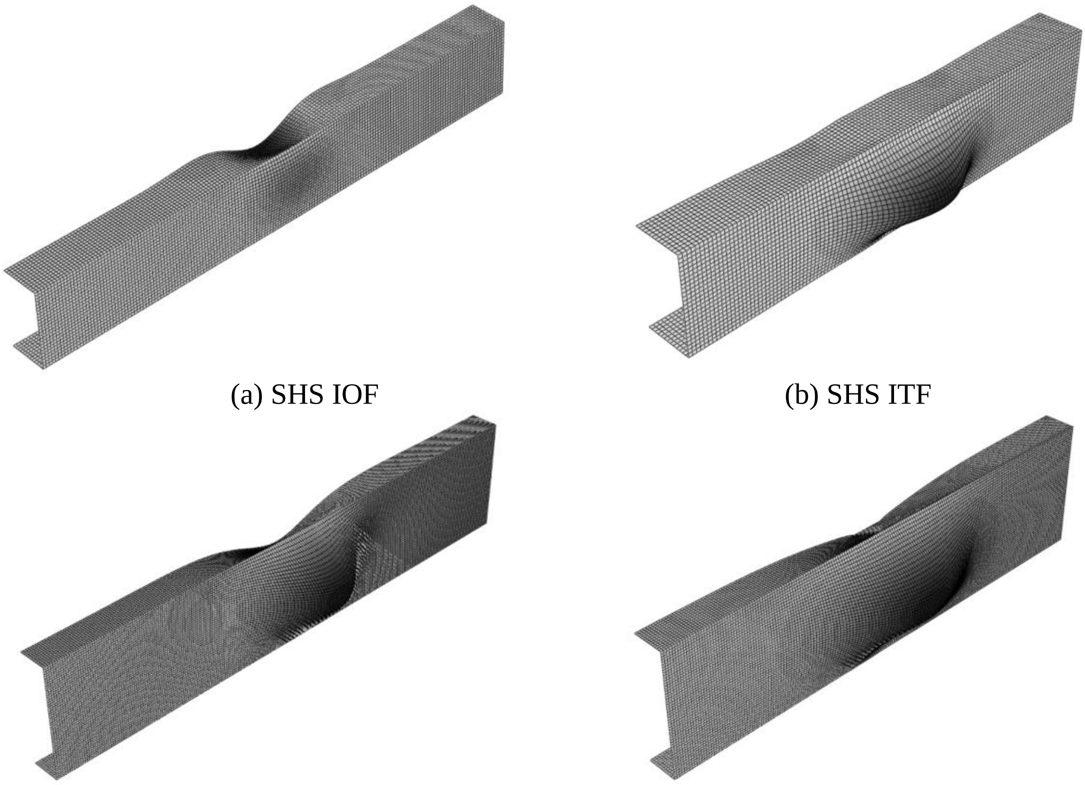

(a) SHS IOF (b) SHS ITF

(c) RHS IOF (d) RHS ITF

Figure 11. Web buckling modes achieved by (a) SHS under IOF, (b) SHS under ITF, (c) RHS under IOF and (d) RHS under ITF with a bearing length of 25 mm

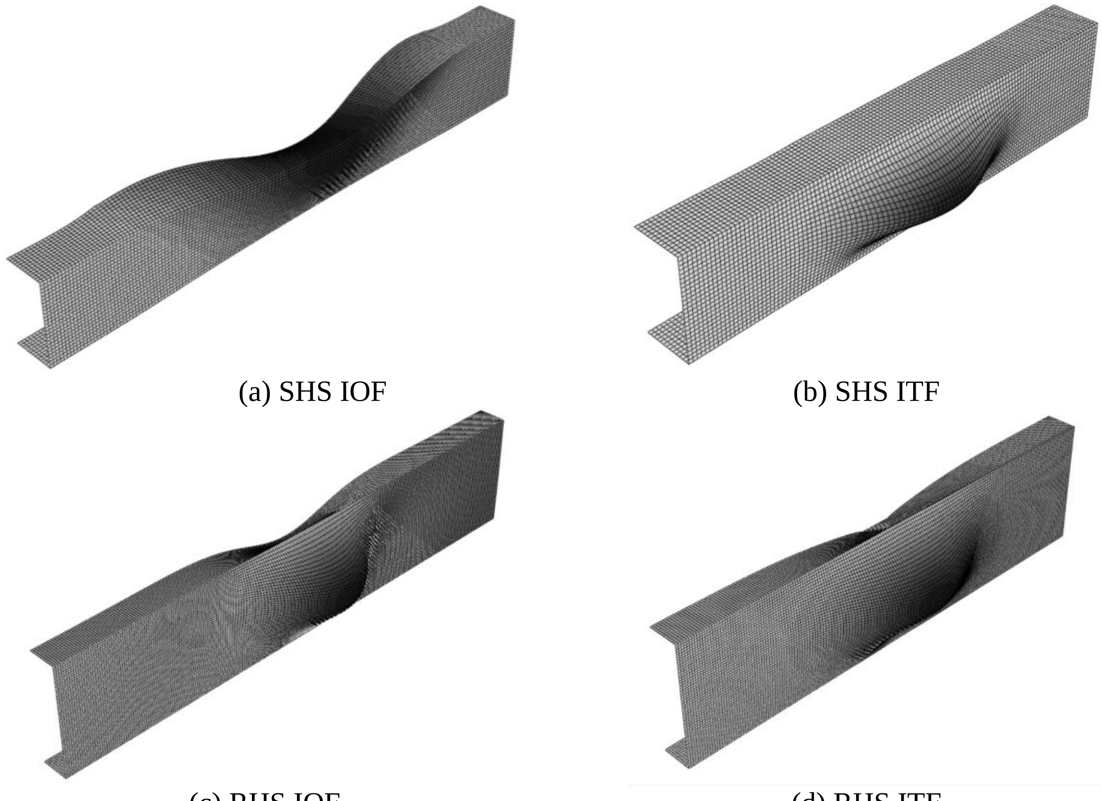

(a) SHS IOF (b) SHS ITF

(c) RHS IOF (d) RHS ITF

Figure 12. Web buckling modes achieved by (a) SHS under IOF, (b) SHS under ITF, (c) RHS under IOF and (d) RHS under ITF with a bearing length of 75 mm

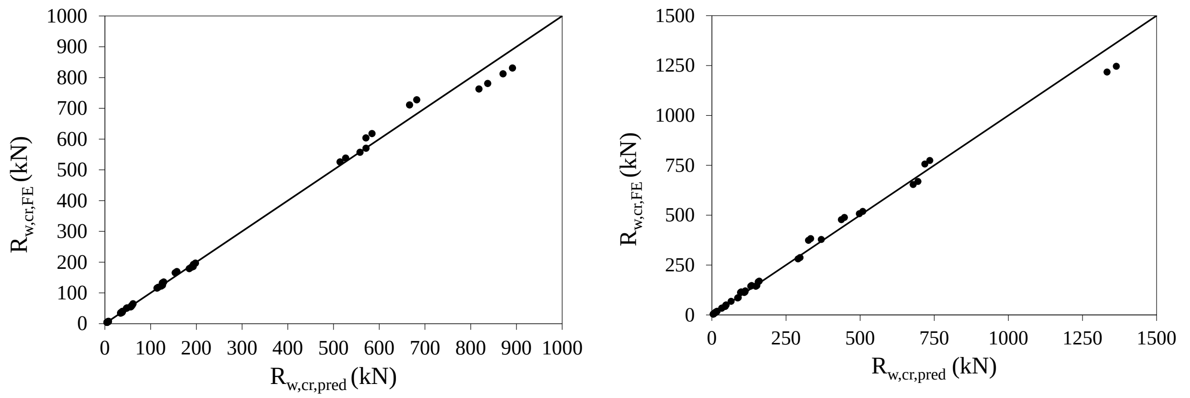

(a) (b)

Figure 13. Comparison between elastic buckling loads numerically obtained $R_{w,cr,FE}$ and predicted by the derived model $R_{w,cr,pred}$ for (a) IOF loading and (b) ITF loading

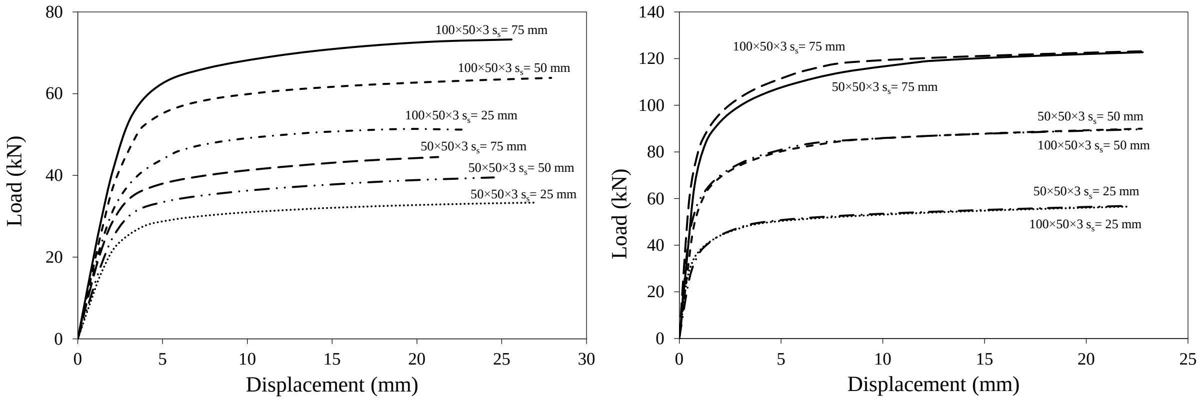

(a) (b)

Figure 14. Load-displacement response from first order plastic analysis for (a) IOF loading and (b) ITF loading

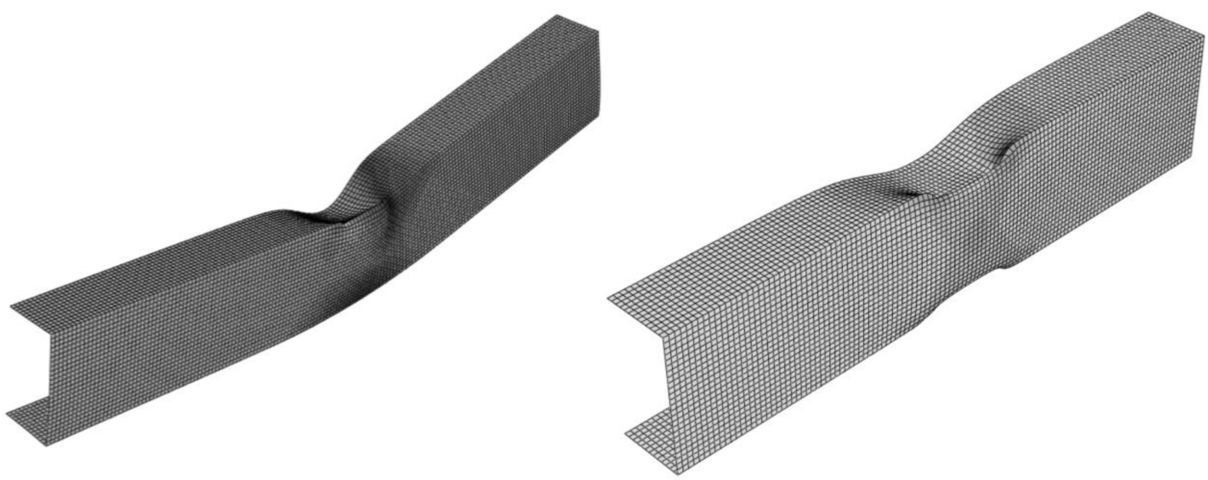

50×50×1 s_s=25 IOF 50×50×3 s_s=25 ITF

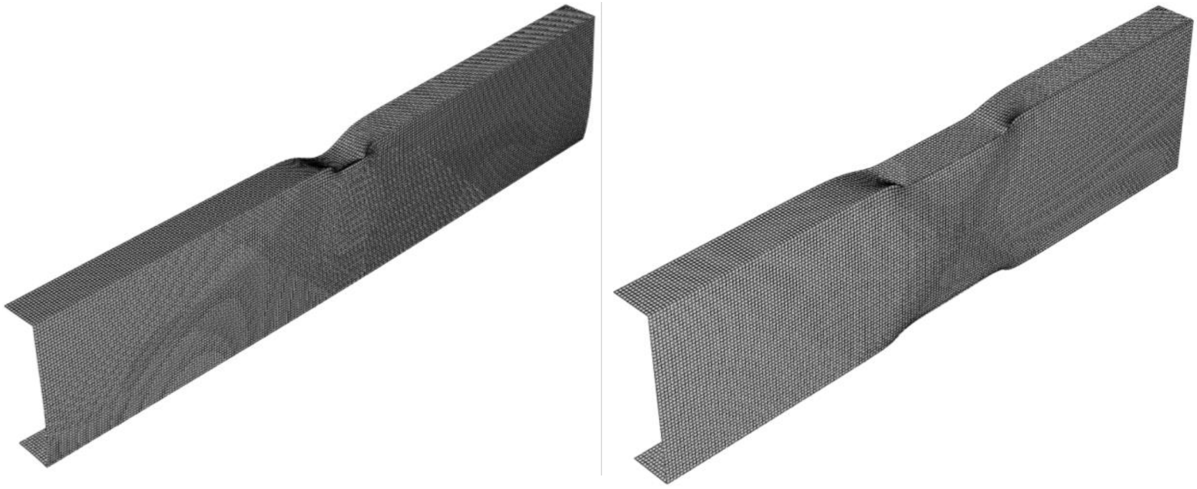

100×50×1 s_s=25 IOF 100×50×5 s_s=75 ITF

Figure 15. Plastic mechanisms developed

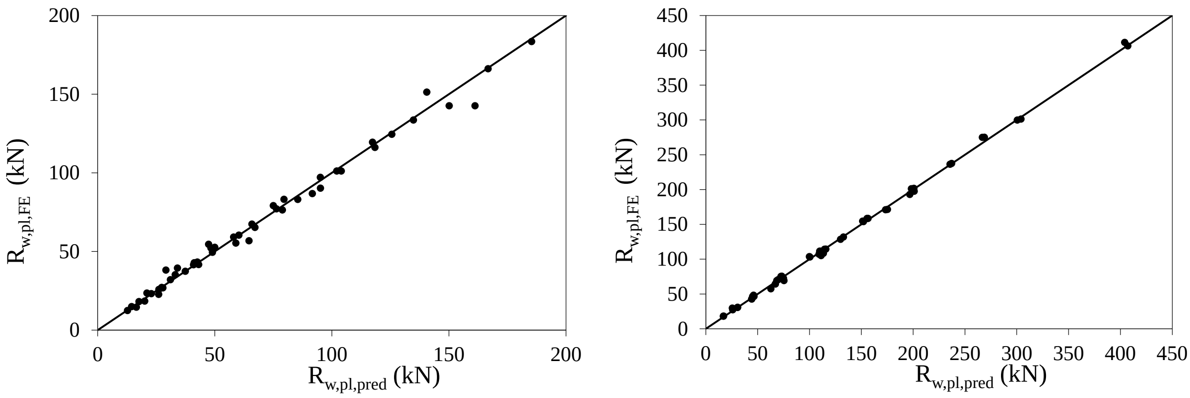

(a) (b)

Figure 16. Comparison between plastic loads numerically obtained $R_{w,pl,FE}$ and predicted by the derived model $R_{w,pl,pred}$ for (a) IOF loading and (b) ITF loading

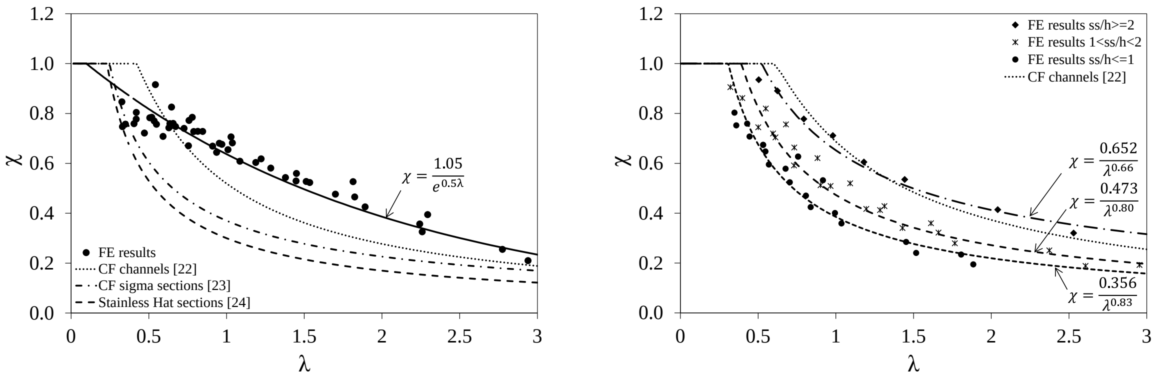

(a) (b)

Figure 17. Numerical results plotted in a $\chi(\lambda)$ space for (a) IOF and (b) ITF loading

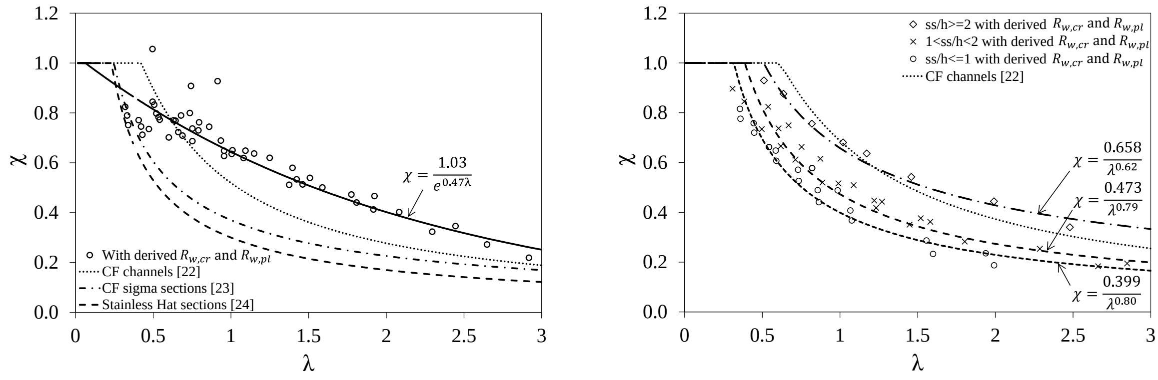

(a) (b)

Figure 18. $\chi(\lambda)$ curves incorporating predictive models $R_{w,cr,pred}$ and $R_{w,pl,pred}$ for (a) IOF and (b) ITF loading

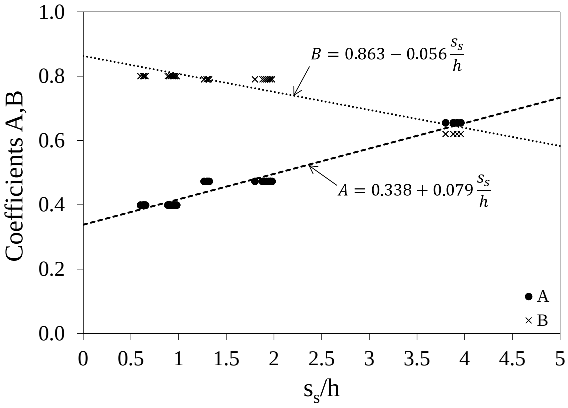

Figure 19. Coefficients A and B from $\chi(\lambda)$ model as a function of s_s/h for ITF loading

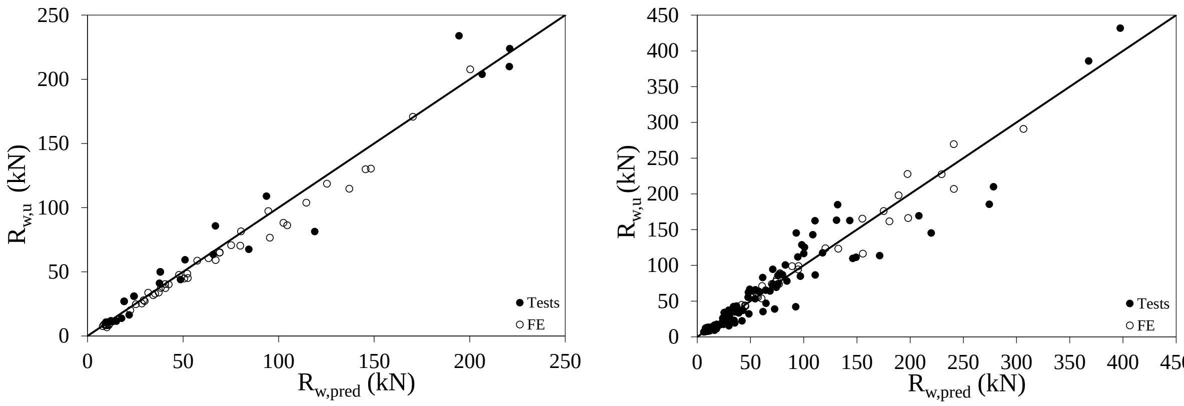

(a) (b)

Figure 20. Comparison between FE/experimental ultimate web crippling resistances and predicted ones by the proposed method for (a) IOF and (b) ITF loading